

Light clusters in warm stellar matter: calibrating the cluster couplings

Tiago Custódio¹, Alexandre Falcão¹, Helena Pais¹, Constança Providência¹, Francesca Gulminelli², and Gerd Röpke^{3,4}

¹ CFisUC, Department of Physics, University of Coimbra, 3004-516 Coimbra, Portugal

² Normandie Univ., ENSICAEN, UNICAEN, CNRS/IN2P3, LPC Caen, F-14000 Caen, France

³ Institut für Physik, Universität Rostock, D-18051 Rostock, Germany

⁴ National Research Nuclear University (MEPhI), 115409 Moscow, Russia

Received: date / Revised version: date

Abstract. The abundances of light clusters within a formalism that considers in-medium effects are calculated using several relativistic mean-field models, with both density-dependent and density-independent couplings. Clusters are introduced as new quasiparticles, with a modified coupling to the scalar meson field. A comparison with experimental data from heavy ion collisions allows settling the model dependence of the results and the determination of the couplings of the light clusters to the meson fields. We find that extra experimental constraints at higher density are needed to convincingly pin down the density associated to the melting of clusters in the dense nuclear medium. The role of neutron rich clusters, such as ${}^6\text{He}$, in asymmetric matter is discussed.

PACS. XX.XX.XX No PACS code given

1 Introduction

Below saturation density, nuclear matter is supposed to undergo a liquid-gas phase transition [1, 2, 3]. Since in physical systems nuclear matter is electrically charged, the phase separation will produce clusterized matter. This behavior is directly reflected in several astrophysical sites, like core-collapse supernovae [4, 5, 6, 7, 8], neutron star (NS) mergers [9, 10, 11], and the inner crust of neutron stars [12, 13, 14]. The form of the clusterized matter depends on temperature and isospin asymmetry. In cold catalysed beta-equilibrium matter, as the one occurring in neutron stars, spherical clusters are found in almost the whole inner crust region, and close to the crust-core transition, the competition between surface and Coulomb forces gives rise to cluster configurations of different geometries coined “pasta phases” [12]. These types of clusters may survive even at finite temperature [15, 16, 17, 18, 19, 20]. Light clusters, i.e. light nuclei like deuterons or α -particles, will form in warm stellar matter as found in core-collapse supernova matter, proto-neutron stars or binary neutron star mergers, and may also coexist with heavy clusters at densities above 10^{-2} fm^{-3} , if the temperature does not overcome a few MeV. The presence of light clusters affects the rates of the reactions involving the weak force, and therefore, may impact the supernova dynamics [4, 21]. In the NS merger evolution, the α particles play an im-

portant role on the dissolution of the remnant torus of accreted matter that surrounds the central high-mass NS formed after the merging. Matter from this accretion disk is also contributing to the ejecta that originates the kilonova observation [10, 11, 22].

Clusterized warm matter at low densities has been described within a generalization of the relativistic mean-field (RMF) approach. Within this framework, light clusters are included as independent degrees of freedom that interact with the medium through their coupling to the mesonic fields [23, 24, 25, 26, 27, 28]. In previous papers [29, 30], some of the present authors introduced a new formalism, that takes into account in-medium effects for the calculation of the equation of state with light clusters for applications in astrophysical systems. These effects are introduced via the scalar cluster-meson coupling, and also via an extra term that is added to the total binding energy of the clusters. This term not only avoids double counting of single particle continuum states, but also affects the dissolution of clusters at high densities. In both references, the studies have been developed within the FSU model [31], which has been fitted to both static and dynamic properties, and it is adequate to describe nuclear matter at saturation density and below. This model, however, is too soft and does not describe neutron stars with two solar masses. It is, therefore, necessary to generalize the previous studies to other models currently used with success to describe symmetric and asymmetric nuclear matter.

Correspondence to: Helena Pais, hpais@uc.pt

Some RMF models are frequently used in simulations and in the study of astrophysical observations, such as the RMF models with non-linear mesonic terms TM1 [32,33] and its modifications [34,35,36,37], NL3 [38] and its modifications [39,36], SFHo [40], FSU2R [41], and RMF with density dependent couplings, like DD2 [25] and DDME2 [42]. Models such as TM1 and NL3 have been fitted to the ground state properties of nuclei. However, they both present a too large slope of the symmetry energy at saturation, far from what the experimental constraints [43,44,45], or ab-initio chiral effective field theory calculations (CEFT) [46], indicate, and, therefore, they have been modified by a non-linear $\omega\rho$ term that smoothens the density dependence of the symmetry energy [39,34,35,36,37]. The parametrization FSU2R [41] is based in the FSU model, which was modified in order to be able to describe two solar mass stars and still to satisfy CEFT results.

In [29,30], it was found that the equilibrium constants determined from the NIMROD data [47] could be well described taking a universal coupling of the σ -meson to all the light clusters considered. Having in mind the inclusion of light clusters in other RMF models besides FSU, it is important to study their behavior at low densities when matter is clusterized and light clusters have an important role in the definition of the transport properties of matter.

In this paper, we want to apply the generalized RMF (gRMF) formalism to low density clusterized matter, where clusters are treated as new quasiparticles, but with a modified coupling to the σ meson field developed in [29,30], using different relativistic mean field models, to understand how they behave. For that matter, we have chosen models with both density-dependent and density-independent couplings. We consider the four usual light clusters, that is, ${}^2\text{H}$, ${}^3\text{H}$, ${}^3\text{He}$, and ${}^4\text{He}$, and we add, inspired by the work done in Ref. [29], another cluster, ${}^6\text{He}$, to our calculations. This cluster has been included in the analysis of the INDRA collaboration [48], which has recently published a new set of equilibrium constants [48] with a controlled bayesian determination of the system density during the expansion, including the possibility of in-medium modifications [49,50]. Note that this gRMF approach has been applied recently also to the description of yields of clusters produced at ternary fission [51].

The aim of the work is to compare different approaches for the RMF parametrization, the description of the coupling to the meson field, and the comparison with the recent INDRA data to investigate the influence of correlations on the equation of state. This comparison serves as criterion to validate different models for the composition of subsaturation nuclear matter.

This paper is organized as follows: a brief summary of the formalism applied is given in the next Section, some results are shown in Section 3, and, finally, in Section 4, some conclusions are drawn.

2 Formalism

We briefly review the RMF models that will be considered in the present work, in particular, FSU2R [41], NL3 $\omega\rho$

Table 1. A few symmetric nuclear matter properties for the models used in this work, calculated at saturation density, n_0 : the binding energy per particle B/A , the incompressibility K , the symmetry energy E_{sym} , the slope of the symmetry energy L , and the nucleon effective mass M^* . All quantities are in MeV, except for n_0 that is given in fm^{-3} , and for the effective nucleon mass that is normalized to the nucleon mass M .

| Model | n_0 | B/A | K | E_{sym} | L | M^*/M |
|------------------|-------|--------|-----|------------------|-----|---------|
| FSU2R | 0.15 | -16.28 | 238 | 30.7 | 47 | 0.59 |
| NL3 $\omega\rho$ | 0.148 | -16.24 | 270 | 31.7 | 55 | 0.60 |
| TM1 $\omega\rho$ | 0.145 | -16.26 | 280 | 31.6 | 56 | 0.63 |
| SFHo | 0.158 | -16.19 | 245 | 31.6 | 47 | 0.76 |
| DDME2 | 0.152 | -16.14 | 251 | 32.3 | 51 | 0.57 |
| DD2 | 0.149 | -16.02 | 243 | 32.7 | 58 | 0.56 |

[36], TM1 $\omega\rho$ [36], SFHo [40], DDME2 [42], and DD2 [25]. In Table 1, we show some symmetric nuclear matter properties calculated at saturation density for these models.

These properties are obtained from the Lagrangian density, that describes nucleons with vacuum mass M coupled to the scalar meson σ with mass m_σ , the vector isoscalar meson ω with mass m_ω and the vector isovector meson ρ with mass m_ρ ,

$$\mathcal{L} = \sum_{i=p,n} \mathcal{L}_i + \mathcal{L}_\sigma + \mathcal{L}_\omega + \mathcal{L}_\rho + \mathcal{L}_{\sigma\omega\rho}, \quad (1)$$

where \mathcal{L}_i is

$$\mathcal{L}_i = \bar{\psi}_i [\gamma_\mu i D^\mu - M^*] \psi_i,$$

with $iD^\mu = i\partial^\mu - g_\omega\omega^\mu - \frac{g_\rho}{2}\boldsymbol{\tau} \cdot \boldsymbol{\rho}^\mu$, and the Dirac effective mass, $M^* = M - g_\sigma\sigma$. The mesonic Lagrangian densities are given by:

$$\begin{aligned} \mathcal{L}_\sigma &= \frac{1}{2} \left(\partial_\mu \sigma \partial^\mu \sigma - m_\sigma^2 \sigma^2 - \frac{1}{3} \kappa \sigma^3 - \frac{1}{12} \lambda \sigma^4 \right), \\ \mathcal{L}_\omega &= -\frac{1}{4} \Omega_{\mu\nu} \Omega^{\mu\nu} + \frac{1}{2} m_\omega^2 \omega_\mu \omega^\mu + \frac{\zeta}{4!} \zeta g_\omega^4 (\omega_\mu \omega^\mu)^2, \\ \mathcal{L}_\rho &= -\frac{1}{4} \mathbf{B}_{\mu\nu} \cdot \mathbf{B}^{\mu\nu} + \frac{1}{2} m_\rho^2 \boldsymbol{\rho}_\mu \cdot \boldsymbol{\rho}^\mu + \frac{\xi}{4!} g_\rho^4 (\boldsymbol{\rho}_\mu \boldsymbol{\rho}^\mu)^2, \end{aligned} \quad (2)$$

where $\Omega_{\mu\nu} = \partial_\mu \omega_\nu - \partial_\nu \omega_\mu$, $\mathbf{B}_{\mu\nu} = \partial_\mu \boldsymbol{\rho}_\nu - \partial_\nu \boldsymbol{\rho}_\mu - g_\rho (\boldsymbol{\rho}_\mu \times \boldsymbol{\rho}_\nu)$, and $\boldsymbol{\tau}$ are the SU(2) isospin matrices.

The Lagrangian density of the models FSU2R, NL3 $\omega\rho$, TM1 $\omega\rho$ and SFHo includes non-linear mesonic terms, which are either self-interaction terms, or terms that mix the σ , ω , and ρ mesons [40]:

$$\mathcal{L}_{\sigma\omega\rho} = g_\rho^2 f(\sigma, \omega_\mu \omega^\mu) \boldsymbol{\rho}^\mu \cdot \boldsymbol{\rho}_\mu, \quad (3)$$

where f is given by

$$f(\sigma, \omega_\mu \omega^\mu) = \sum_{i=1}^6 a_i \sigma^i + \sum_{j=1}^3 b_j (\omega_\mu \omega^\mu)^j \quad (4)$$

for SFHo, and by

$$f(\sigma, \omega_\mu \omega^\mu) = \Lambda_v g_v^2 \omega_\mu \omega^\mu \quad (5)$$

for FSU2R, NL3 $\omega\rho$ and TM1 $\omega\rho$.

The models DD2, DDME2 have density-dependent couplings and no nonlinear mesonic terms. Their isoscalar couplings of the mesons i to the baryons are given by

$$g_i(n_B) = g_i(n_0) a_i \frac{1 + b_i(x + d_i)^2}{1 + c_i(x + d_i)^2}, \quad i = \sigma, \omega, \quad (6)$$

and the isovector meson-nucleons coupling by

$$g_\rho(n_B) = g_\rho(n_0) \exp[-a_\rho(x - 1)]. \quad (7)$$

In the last expressions, n_0 is the model-dependent symmetric nuclear saturation density, see Tab. 1, and $x = n_B/n_0$, with n_B the baryonic density.

In order to include explicitly the light clusters as constituents of nuclear matter, we consider them as point like particles, neglecting intrinsic structures. This approximation is acceptable at low densities when the volume accessible to each clusters is much larger than its volume. In RMF approach they will interact with the medium through their coupling to the mesons. We add to the Lagrangian density the cluster contributions, and for homogeneous matter each one contributes to the total energy density of the system with

$$\mathcal{E}_i = \frac{2S^i + 1}{2\pi^2} \int k_i^2 E_i(f_{i+}(k) + f_{i-}(k)) dk + g_{i\omega} \omega^0 n_i + g_\rho \rho_3^0 I_3^i n_i, \quad (8)$$

where $E_i = \sqrt{k_i^2 + M_i^{*2}}$ is the cluster single-particle energy, and M_i^* the effective mass of cluster i . The cluster spin, isospin and density are denoted, respectively, by S^i , I_3^i , and n_i . The distribution functions for the particles and antiparticles $f_{i\pm}$ are defined as

$$f_{i\pm} = \frac{1}{\exp[(E_i \mp \nu_i)/T] + \eta}, \quad (9)$$

with $\eta = 1$ for fermions and $\eta = -1$ for bosons, T the temperature, and $\nu_i = \mu_i - g_{i\omega} \omega^0 - g_\rho I_3^i \rho_3^0$. The coupling of the clusters to the ω -meson is given by $g_{i\omega} = A_i g_\omega$, with A_i the cluster mass number.

We define the binding energy of the cluster i in the medium as in [29]

$$B_i = A_i m^* - M_i^*, \quad i = d, t, h, \alpha, {}^6\text{He}, \quad (10)$$

with M_i^* given by

$$M_i^* = A_i m - g_{i\sigma} \sigma_0 - (B_i^0 + \delta B_i). \quad (11)$$

In this last expression, B_i^0 is the binding energy of the cluster in the vacuum, which will be fixed to the experimental values, the second term denotes the coupling of the cluster to the σ -meson, and the last term describes a binding energy shift. In the following, we will write the coupling $g_{i\sigma}$ in terms of the coupling of the nucleon to the σ -meson, g_σ , as $g_{i\sigma} = x_s A_i g_\sigma$, with x_s its fraction, ranging from 0 to 1, to modify (decrease) the nuclear attraction. For the binding energy shift δB_i , we consider [29, 52, 53]

$$\delta B_i = \frac{Z_i}{n_0} (\epsilon_p^* - m n_p^*) + \frac{N_i}{n_0} (\epsilon_n^* - m n_n^*), \quad (12)$$

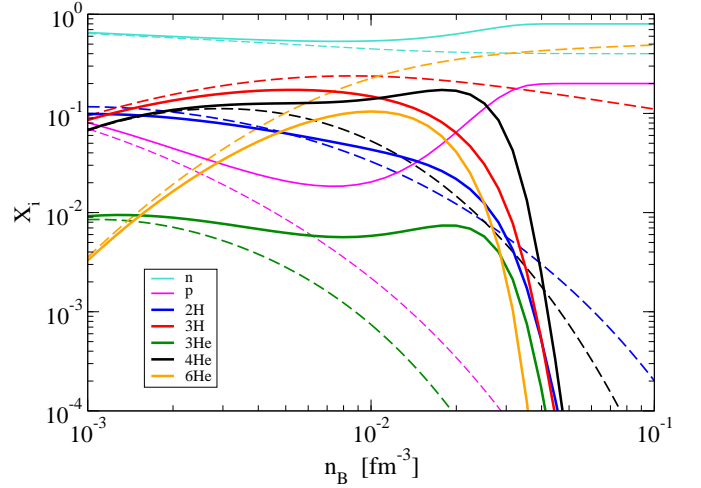


Fig. 1. (Color online) The abundances (mass fraction) of the stable isotopes n, p, d, t, h, α , and ${}^6\text{He}$ considered as a function of the density for $T = 5$ MeV and a fixed proton fraction of 0.2. The NSE (dashed) is compared to a QS calculation (full lines), see text.

where the gas energy density ϵ_j^* and nucleonic density n_j^* , $j = n, p$, are given by [29]

$$\epsilon_j^* = \frac{1}{\pi^2} \int_0^{k_{F_j}(\text{gas})} k^2 E_j(f_{j+}(k) + f_{j-}(k)) dk \quad (13)$$

$$n_j^* = \frac{1}{\pi^2} \int_0^{k_{F_j}(\text{gas})} k^2 (f_{j+}(k) + f_{j-}(k)) dk, \quad (14)$$

with $k_{F_j}(\text{gas}) = (3\pi^2 n_j)^{1/3}$ defined using the zero temperature relation between density and Fermi momentum. This was proposed in [29] as an effective way of implementing Pauli blocking in a range of temperatures for which the Fermi distribution is close to a step function. These two quantities, ϵ_j^* and n_j^* , define the energy density and the density of nucleon j associated to the levels below the Fermi momentum, $k_{F_j}(\text{gas})$, of the $T = 0$ nucleonic density n_j . The term δB_i can be identified as an excluded volume mechanism in the Thomas-Fermi approximation. The gRMF model is able to describe the occurrence of clusters in nuclear matter and density modifications. The parameters are introduced in an empirical way, and it is our goal to discuss different choices for these parameters, in particular the coupling of clusters x_s to the σ -meson. There are also alternatives to describe density effects such as the excluded volume concept, see [6], which also uses empirical parameters. A microscopic, quantum statistical approach can be given, see [54] and references therein, which, however, is not simple to be used for practical applications.

3 Results

Before comparing different gRMF models, we give a general discussion of the problem to include correlations and

cluster formation in the EoS. In Fig. 1, the mass fraction $X_i = A_i n_i / n_B$ for the stable isotopes $i = n, p, d, t, h, \alpha$, and ${}^6\text{He}$ is shown for $T = 5$ MeV, $y_p = 0.2$ in the baryon number density region $0.001 \text{ fm}^{-3} < n_B < 0.1 \text{ fm}^{-3}$; y_p is the fixed global proton fraction, and n_i the particle number density. We have $\sum_i X_i = 1$. The calculation of the composition according to the simple model of nuclear statistical equilibrium (NSE) neglecting all interactions between the constituents, and considering only the ground states of the stable isotopes, is compared to a quantum statistical (QS) calculation taking in-medium effects into account, in particular Pauli blocking and the quasiparticle shift taken as DD2-RMF, see [54]. In the low-density region, the interaction between the constituents of nuclear matter can be neglected so that this limiting region is appropriately described by the NSE. A small difference is observed for the deuteron mass fraction owing to the virial limit which is correctly described by the QS approach. The account of excited states implements also the account of scattering states in the virial EoS [55, 56] which leads to a significant contribution for the deuteron fraction because of its small binding energy. As seen from Fig. 1, in-medium effects become appreciable above $n_B = 10^{-3} \text{ fm}^{-3}$.

The most striking effect is the suppression of bound state abundances because of Pauli blocking so that near the saturation density these clusters nearly disappear, and we obtain a Fermi liquid of neutrons and protons. These are treated as quasiparticles containing a mean-field energy shift. Different versions of these RMF approaches are presented and compared in this work. We have to interpolate between two limiting cases, the virial expansion in the low-density limit and the RMF approach near the saturation density. In particular, the virial EoS depends only on the experimentally determined binding energies and scattering phase shifts [55, 56], and provides at finite temperature the correct zero density limit. The exact microscopic description of the intermediate region is a difficult many-particle problem. Continuum correlations and higher order clustering in a dense medium is hard to calculate within the QS approach. Interpolations are of interest which may be probed by laboratory experiments as shown in this paper.

An interesting issue seen also in Fig. 1 is that within the NSE calculation with a given set of isotopes, the neutron-rich clusters become dominant at increasing density, because the proton fraction is small so that exotic nuclei like ${}^6\text{He}$ are most abundant near the saturation density. We can extend the NSE including resonant states such as ${}^4\text{H}$ and ${}^5\text{He}$. In a recent publication by Yudin et al. [57], it was claimed that these exotic nuclei may be of importance in stellar matter, in particular with respect to the neutrino opacity. However, as shown in Refs. [58, 21], within a more systematic approach the contribution of the resonant states should be expressed in terms of the scattering phase shifts so that their contribution is strongly reduced. Therefore, in this paper, we restrict our calculations only to ${}^6\text{He}$, which is also measured in the INDRA experiment. Within a more exhaustive investigation one can also search for ${}^8\text{He}$ and other clusters, but it is expected that their

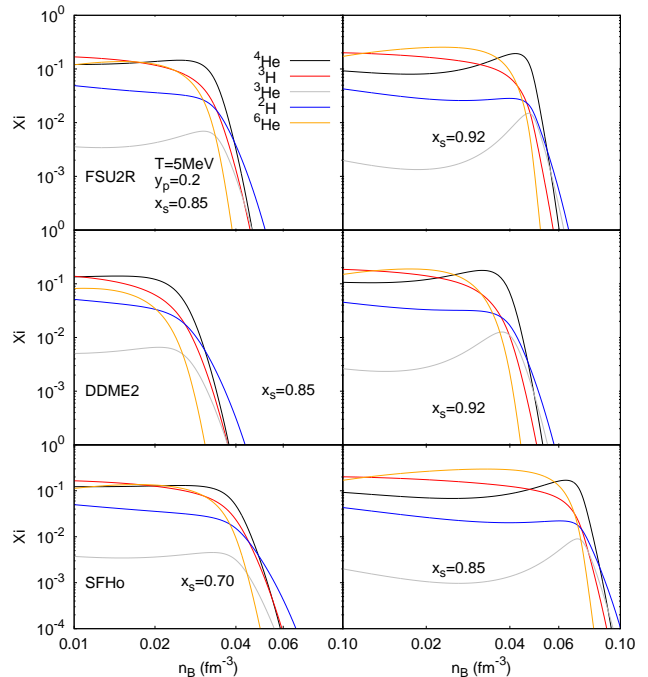


Fig. 2. (Color online) The abundances of all the clusters considered as a function of the density for $T = 5$ MeV and a fixed proton fraction of 0.2 for FSU2R (top), DDME2 (middle), and SFHo (bottom) obtained with $x_s = 0.85$ (left) and $x_s = 0.92$ (right). For the SFHo model, the scalar cluster-meson coupling used was 0.7 and 0.85.

mass fractions are very small. We will not go in more details here, but discuss what can be learned from laboratory experiments to derive adequate interpolation expressions to infer the composition in the whole subnuclear density region.

To this aim, in the present section, we compare the distribution of light clusters at low densities obtained with the models FSU2R, NL3 $\omega\rho$, TM1 $\omega\rho$, SFHo, DDME2, and DD2, and we discuss how well these models describe the equilibrium constants determined from the INDRA [48, 49, 50] data.

As referred before, in [29] it was shown that taking the universal coupling $x_s = 0.85 \pm 0.05$ of the σ -meson to the light clusters d, t, h, α would describe well the equilibrium constants determined from the NIMROD data [47]. These data, however, have been analyzed making the hypothesis that the system volume can be obtained assuming an ideal gas equation of state for the clusters. Recently, the INDRA collaboration [48] has performed a similar experiment with the heavier system Xe-Sn, where different tin and xenon isotopes were used, and considered in the analysis also the ${}^6\text{He}$ cluster, besides the light clusters d, t, h, α . The Bayesian analysis of these data performed in [49, 50], allowing possible in-medium corrections in the determination of the system volume, has shown that a larger value $x_s = 0.92 \pm 0.02$ should be taken for the cluster σ -meson coupling. However, this value is obtained with a specific version of the RMF model, namely FSU, and it could be model dependent. For this reason, in the follow-

ing figures, we will consider different values of x_s for the σ meson-cluster coupling within the RMF models introduced above.

In Fig. 2, we show the mass fractions of all the clusters considered as a function of the density for a temperature of 5 MeV and a fixed proton fraction $y_p = 0.2$. We have chosen three models: two with nonlinear mesonic terms and constant couplings (FSU2R and SFHo), and another with density-dependent couplings (DDME2). We have taken the scalar cluster-meson coupling fraction as 0.85 and 0.92 for both FSU2R and DDME2. For SFHo, we have considered a smaller fraction, 0.7 and 0.85, because taking a larger fraction, e.g. 0.92, would make the dissolution of the clusters occur at a much larger density, as we will see in the following. Moreover, a smaller x_s is necessary to reproduce the virial EoS at low densities, and to fit the equilibrium constants deduced from the INDRA data as will be discussed later. We can see that below $n_B \approx 3 \times 10^{-2} \text{ fm}^{-3}$, the most abundant clusters are ${}^3\text{H}$, ${}^4\text{He}$, and ${}^6\text{He}$. This is because the clusters ${}^6\text{He}$ and ${}^3\text{H}$ are the neutron-richest ones, and we are considering asymmetric neutron rich matter, and ${}^4\text{He}$ is the most bound one. The heaviest cluster ${}^6\text{He}$ is the first to dissolve while the lightest one ${}^2\text{H}$ is the last one. For FSU2R and SFHo, ${}^6\text{He}$ is the most abundant cluster in a short range of densities taking, respectively, $x_s = 0.85$ and 0.7. It is striking that for $x_s = 0.92$ (0.85) for FSU2R (SFHo), ${}^6\text{He}$ becomes the most abundant in the range 0.01 to 0.04 fm^{-3} . Within DDME2, the clusters dissolve at the smallest densities, and ${}^6\text{He}$ is the most abundant cluster in a short range of densities only when the larger value of x_s is considered. For $x_s=0.85$, the dissolution density range for all clusters is $\sim 4 - 6 \times 10^{-2} \text{ fm}^{-3}$ for FSU2R and DDME2. It is interesting to see that for the RMF with non-linear terms, such as FSU2R and SFHo, the fraction of ${}^6\text{He}$ clusters becomes quite large just before the binding energy of the cluster goes to zero, followed by a steep decrease of the abundance of this cluster. In the case of SFHo and $x_s=0.85$, we can even identify a first order phase transition at this density.

In Fig. 3, we compare the α -particle mass distributions obtained for the models FSU2R, NL3 $\omega\rho$, TM1 $\omega\rho$, SFHo, DD2 and DDME2, considering a temperature of $T = 10$ MeV, and proton fraction of $y_p = 0.41$. For all the models shown, the scalar cluster-meson coupling fraction is set to $x_s=0.85$. For SFHo, we have also plotted the abundances with $x_s = 0.70 \pm 0.05$, represented by the hashed region. The differences reflect the properties of these models at subsaturation densities. Below 0.02 fm^{-3} , i.e. not far from the range of densities where the virial EoS is valid, all models give similar results. Above 0.03 fm^{-3} , the models start to differ, with DD2 and DDME2 predicting the smallest dissolution density, slightly below 0.05 fm^{-3} , and SFHo the largest one, $\approx 0.1 \text{ fm}^{-3}$. SFHo is, in fact, a special case because all the other models predict dissolution densities in a narrow range of $\sim 0.05 - 0.06 \text{ fm}^{-3}$. With SFHo, we get a similar result, if the x_s is reduced to $\approx 0.65 - 0.7$. It is expectable that under the conditions where light clusters play an important role, the predictions

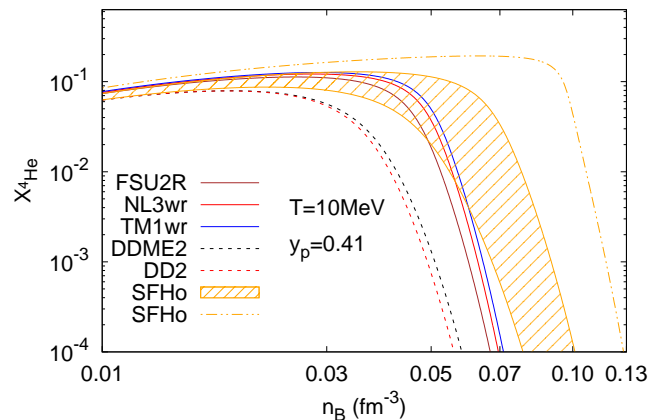


Fig. 3. (Color online) The mass fraction of the α cluster as a function of the density for all the models considered, and $T = 10$ MeV. The scalar cluster-meson coupling fraction is set to $x_s = 0.85$, except for SFHo where the results are shown for $x_s = 0.7 \pm 0.05$ (wide hashed band) and for $x_s = 0.85$ (dash-dotted-line). The proton fraction is fixed at 0.41.

obtained with SFHo will differ from the ones obtained with any of the other five models. This could be expected from the results of Ref. [59] where the spinodal sections obtained for SFHo extend to a much larger (n_p, n_n) phase-space region than FSU2R, TM1 $\omega\rho$ or DDME2.

In Fig. 4, we plot, for comparison, the mass distributions of the five clusters considered, calculated within the models FSU2R, NL3 $\omega\rho$, TM1 $\omega\rho$, SFHo, DD2 and DDME2, for two temperatures, $T = 5$, and 10 MeV, and two proton fractions $y_p = 0.2$ and 0.41. The temperatures chosen are typical in proto-neutron stars, and the proton fractions reflect two different stages of the star evolution. Some general comments are in order: (i) In average, models with density-dependent couplings give different fractions from the others if the same value of x_s is chosen. They generally predict the cluster dissolution at smaller densities and smaller particle fractions at low densities for the neutron rich clusters; (ii) In the low-density range shown, the neutron rich clusters, tritium and ${}^6\text{He}$, are the most abundant clusters for $y_p = 0.2$ and $T = 5$ MeV. At $T = 10$ MeV, this is still true for the tritium, the one with the smallest mass; (iii) Models with non-linear mesonic terms show a steeper behavior close to the dissolution density.

We now turn to examine how the differences observed in the models reflect in the predictions for the equilibrium constants, which are the quantities determined from the experimental data [47,48]. The equilibrium constants are defined as the ratio

$$K_{ci} = \frac{n_i}{n_n^{N_i} n_p^{Z_i}},$$

where n_i is the density of cluster i , n_n and n_p are, respectively, the density of free neutrons and protons, and Z_i , N_i are the number of protons and neutrons in cluster i .

In Fig. 5, we plot the equilibrium constants obtained with the different models on typical $(n_B - T)$ trajectories

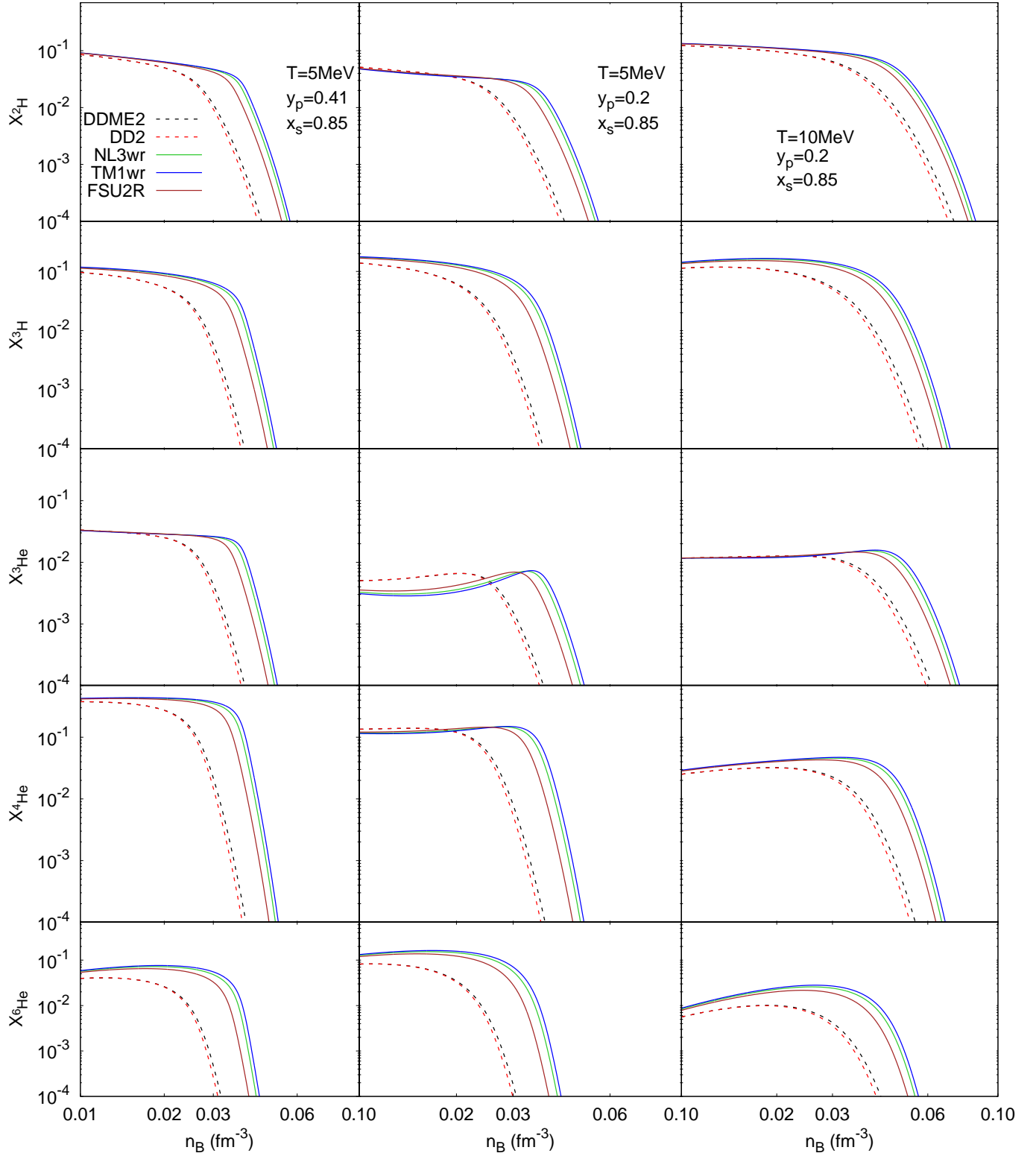


Fig. 4. (Color online) The mass abundances of all the clusters considered as a function of the density for the models FSU2R, NL3 $\omega\rho$, TM1 $\omega\rho$, SFHo, DD2 and DDME2 and $T = 5$ MeV and $y_p = 0.41$ (left column), $T = 5$ MeV and $y_p = 0.2$ (middle column), and $T = 10$ MeV and $y_p = 0.2$ (right column). In all calculations, the scalar cluster-meson coupling is set to $x_s = 0.85$.

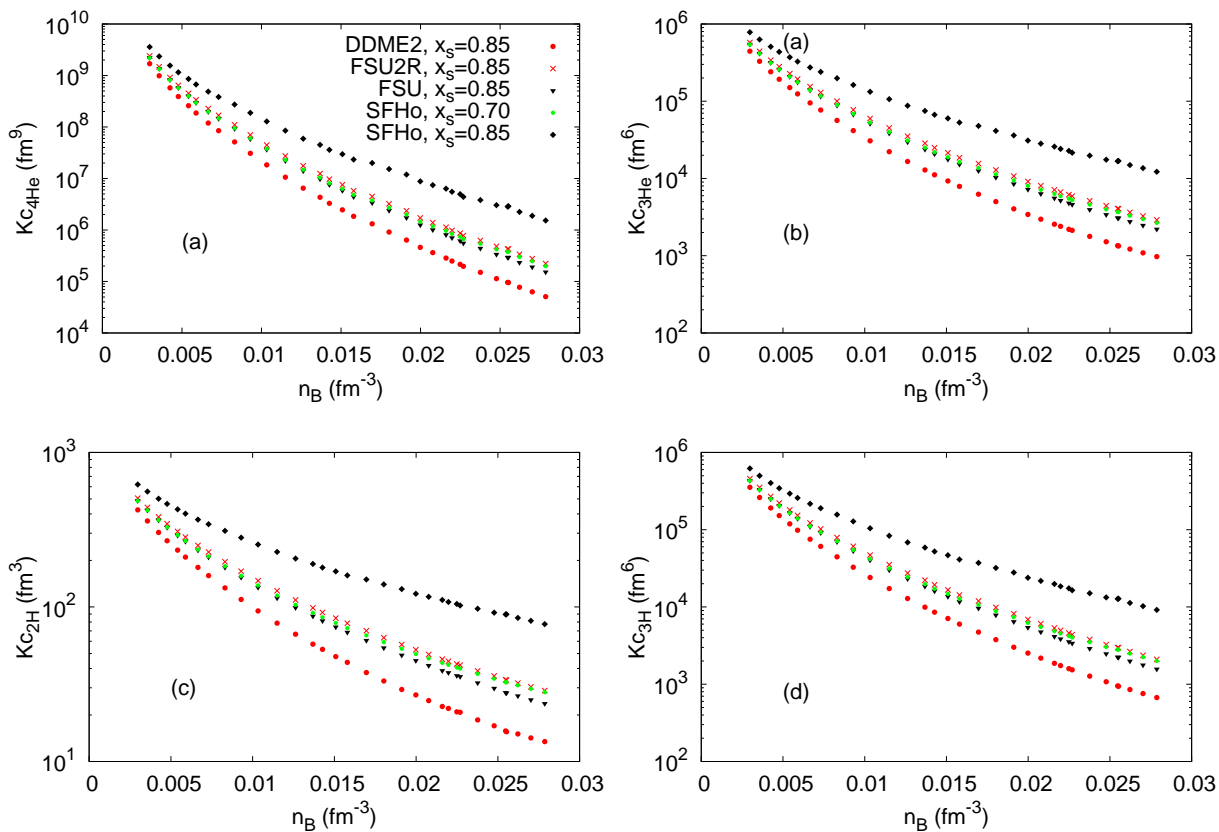


Fig. 5. (Color online) The chemical equilibrium constants as a function of the density from a calculation where we consider homogeneous matter with four light clusters for the DDME2 (red circles), FSU2R (crosses), and FSU (black triangles) models, calculated at the experimental values (T , $n_{B\text{exp}}$, $y_{p\text{exp}} = 0.41$) proposed in Ref. [47], and considering the cluster coupling as $x_s = 0.85$. Also shown are the results for SFHo with $x_s = 0.7$ (yellow circles) and $x_s = 0.85$ (black diamonds).

that can be explored in heavy ion collisions. The choice of the temperature value, at each density point, is the one estimated in Ref. [47], and the proton fraction is fixed to $y_p = 0.41$ at each point. The volume estimation in that paper is not fully realistic, since it was made in the simplifying assumption of an ideal cluster gas. However, many different theoretical calculations [60] were produced assuming the (T, n_B, y_p) correlation of Ref. [47], therefore this particular choice is useful to assess the model dependence of the calculations. In this Figure, the sensitivity of the chemical constants to the scalar cluster-meson coupling for one representative model, SFHo, is shown. We can see that the effect previously observed in Fig. 3, namely the positive correlation between the value of x_s , here reflects into higher values for the equilibrium constants when x_s is increased. This effect is sizeable and potentially bigger than the experimental error bars on equilibrium constants, meaning that a comparison with experimental data, within a given model, allows predicting the dissolution density of clusters in dense matter. The results of three different models DDME2, FSU2R and SFHo, using the same value for that coupling, fixed to $x_s = 0.85$, as proposed in [29], are also displayed in this figure, and they show the model dependence of the equilibrium constant prediction. Models $\text{TM}1\omega\rho$ and $\text{NL}3\omega\rho$ have a behavior

very close to FSU2R, and are not represented. The difference between the predictions is a measure of the model dependence of the calculation. We can see that the chemical constants are smaller for DDME2 reflecting the fact discussed before that the clusters dissolve at smaller densities within this model. We can, however, say that the behavior of FSU2R and DDME2 models is similar to the one obtained in [29] within the model FSU, probably due to the fact that these models have similar properties at subsaturation densities.

As expected, the coupling x_s is model-dependent, and it should be fitted to some experimental data or ab-initio calculation. In the following, we determine for each model the range of x_s values that best reproduces the INDRA equilibrium constants for the different clusters as calculated in [49]. In Fig. 6, we show how the chemical equilibrium constants calculated within models FSU2R, DDME2 and SFHo with the best x_s values compare with the ones extracted from the experimental data obtained by the INDRA collaboration. We have obtained for FSU2R $x_s = 0.91 \pm 0.02$, for DDME2 $x_s = 0.93 \pm 0.02$, and for SFHo $x_s = 0.83 \pm 0.03$. It is observed that the quality of the fit depends slightly on the size of the clusters, and this deserves an investigation in a future work. Let us recall that previously, in Refs. [49, 50], the authors performed an

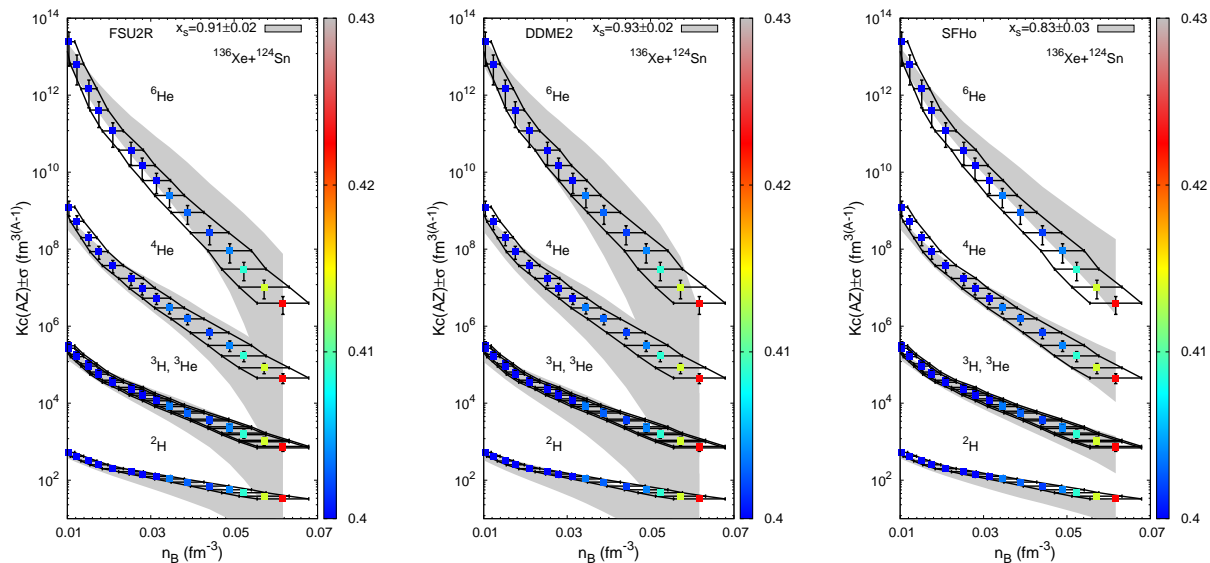


Fig. 6. (Color online) The equilibrium constants as a function of the density. The full lines represent the experimental results of the INDRA collaboration, with 1σ uncertainty. The grey bands are the equilibrium constants from a calculation [30] where we consider homogeneous matter with five light clusters for the FSU2R EoS (left), the DDME2 EoS (middle) and SFHo EoS (right), calculated at the average value of $(T, n_{B,\text{exp}}, y_{p,\text{exp}})$, and considering cluster couplings in the range of $x_s = 0.91 \pm 0.02$ (FSU2R), $x_s = 0.93 \pm 0.02$ (DDME2) and $x_s = 0.83 \pm 0.03$ (SFHo). The color code represents the global proton fraction.

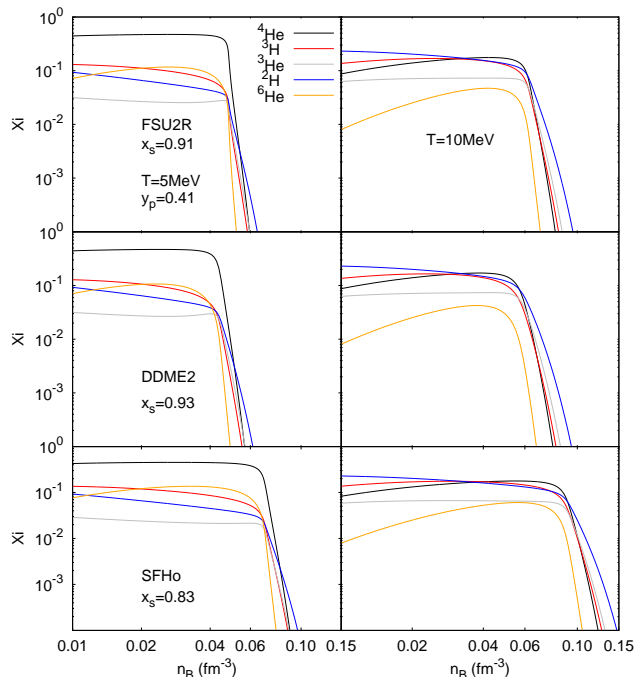


Fig. 7. (Color online) The abundances of all the clusters considered as a function of the density for $T = 5$ MeV (left) and $T = 10$ MeV (right) and a fixed proton fraction of 0.41 for FSU2R with $x_s = 0.91$ (top), DDME2 with $x_s = 0.93$ (middle), and SFHo with $x_s = 0.83$ (bottom).

analysis of the experimental data within the FSU model, and in order to reproduce data, it was necessary to take $x_s = 0.92 \pm 0.02$, a result very close to the one obtained

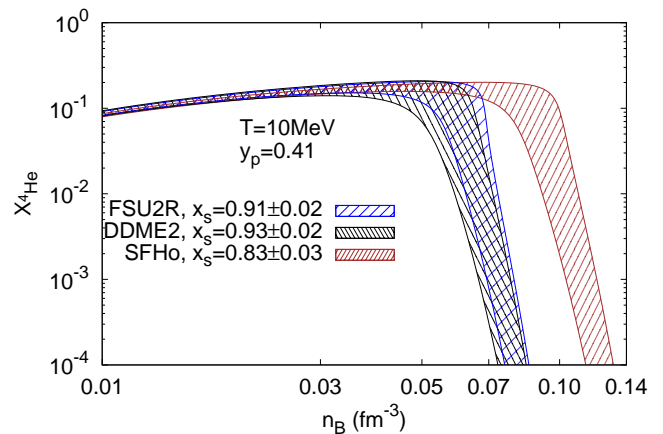


Fig. 8. (Color online) The mass fraction of the α -particle as a function of the density for $T = 10$ MeV and a fixed proton fraction of 0.41 for FSU2R with $x_s = 0.91 \pm 0.02$, DDME2 with $x_s = 0.93 \pm 0.02$, and SFHo with $x_s = 0.83 \pm 0.03$.

with FSU2R and DDME2. For SFHo, and as we saw before, we need a smaller coupling x_s to fit this data.

Choosing the scalar cluster-meson coupling ratio that best fits the INDRA data, we calculate the clusters abundances for FSU2R, DDME2 and SFHo, for $y_p = 0.41$ and $T = 5$ and 10 MeV, see Fig. 7. All models predict similar abundances of all the clusters considered up to a density ≈ 0.05 fm^{-3} for $T = 5$ MeV and ≈ 0.06 fm^{-3} for $T = 10$ MeV. This result is very interesting: in fact, as shown in [50], the INDRA data explore densities up to ≈ 0.06 fm^{-3} , however these larger densities are attained at a temperature ≈ 9 MeV. Matter at $T = 5$ MeV corresponds to

densities below $\approx 0.02 \text{ fm}^{-3}$. We may, therefore, expect that a fit to the INDRA data is giving information on the abundances of light clusters corresponding to a pair (T , n_B). Although the proton fraction is also changing along with T and n_B , it takes values in a very narrow range, 0.39-0.42, very close to $y_p = 0.41$ used to calculate the cluster abundances in Fig. 7.

Models FSU2R and DDME2 show very similar fractions also above $\approx 0.05 \text{ fm}^{-3}$, in particular, at the maximum of the distributions and at the dissolution density, which we define as the density above which the fractions are below 10^{-4} . However, SFHo predicts dissolution densities $\sim 30\%$ larger than the other two models.

Having this in mind, we plot in Fig. 8 the mass fraction of the α -particle as a function of the density for the three models previously considered, and a temperature of 10 MeV and a fixed proton fraction of 0.41. For each model, we choose the range of the σ -coupling that best fits the INDRA data. We confirm that the α -abundances predicted by the three models coincide up to $\approx 0.06 \text{ fm}^{-3}$. Moreover, for FSU2R and DDME2 we do have a complete superposition of the bands, indicating a similar prediction for the dissolution density. SFHo, however, shows a higher dissolution density, $\sim 30\%$ larger.

The present results seem to indicate that a good reproduction of the equilibrium constants obtained from the experimental data could imply a unique prediction for the cluster abundances, and, in particular, of the dissolution density only if we could have some extra experimental constraints at a slightly higher density.

4 Conclusions

We have analyzed the appearance of light clusters in warm non-homogeneous matter at densities below saturation density in the framework of RMF models. We used six models that properly describe nuclear matter properties, and predict stars with more than two solar masses, two of which with density-dependent couplings, and the other four with non-linear mesonic terms. Light clusters were included as point-like particles that are affected by the medium through their couplings to the mesons. For these couplings, we have considered: (a) the results of [29], where, for the σ -meson coupling, a universal coupling proportional to $A_i x_s g_\sigma$, with x_s to be fixed on experimental data, was proposed; (b) the couplings determined in [49, 50] extracted from the INDRA [48] experimental data.

Except for the model SFHo, we have found that different models predict similar abundances of clusters. Overall, for the density-dependent models we have obtained 15% to 20% smaller dissolution densities, but far from the dissolution density, the abundances are similar with respect to the non-linear models. For SFHo, taking the same scalar cluster-meson coupling, the dissolution densities are approximately the double, and the cluster abundances are larger. It is, therefore, expectable that simulations that use SFHo to describe supernova explosions or binary NS mergers will have larger contributions of light clusters. In order to reproduce the equilibrium constants obtained from

heavy ion collisions, a smaller coupling of the light clusters to the σ -meson has to be considered. We conclude that the clusterization effect, in particular the amount and the chemical composition of clusters, depends on the behavior of the model in the corresponding density range. Taking universal couplings for the clusters highlights the differences. The present heavy ion constraints are not enough to distinguish between models like DDME2 and FSU2R, but clearly shows that SFHo requires a different treatment.

In the present comparison, we have considered besides the lighter clusters d , t , h , and α , also the heavier cluster ${}^6\text{He}$. In asymmetric matter, it was shown that the contribution of this cluster is quite important in a range of densities not far from the dissolution density. A discussion of the role of heavier clusters at the densities and temperatures studied in the present work has been presented in [30]. Moreover, we believe there is a need of experimental measurements for heavier clusters in order to discriminate the different models.

The gRMF formalism presented here allows to take cluster formation into account for hot and dense nuclear matter, in particular stellar matter. For the contribution of nucleon quasiparticles (n, p) different parametrizations within the RMF are possible. We considered several models, and some of them were calibrated to the INDRA data, namely FSU2R, DDME2, and SFHo. The coupling parameter x_s for the interaction with the σ field can be introduced as a global quantity for all clusters. It determines the density where the respective clusters are dissolved. We have shown that if x_s is fitted to equilibrium constants determined from experimental data, different models predict similar abundances up to the densities and temperatures explored by INDRA data. The dissolution densities, however, differ: while two of the models, FSU2R and DDME2 predict similar behavior at dissolution, the third model, SFHo, gives dissolution densities that are at least 30% larger. In the future, a more careful analysis will be undertaken using statistical methods to extract these quantities. Besides, a microscopic approach to this coupling parameter may show a dependence on the respective nucleus, as well as on thermodynamic parameters, like the temperature. This may indicate that the model applied in the present study needs to take these dependences into account. This point is left for future developments.

We thank R. Bougault for useful discussions. This work was supported by the FCT (Portugal) Projects No. UID/FIS/04564/2019 and UID/FIS/04564/2020, and POCI-01-0145-FEDER-029912, by PHAROS COST Action CA16214, and by the German Research Foundation (DFG), Grant # RO905/38-1. H.P. acknowledges the grant CEECIND/03092/2017 (FCT, Portugal).

References

1. M. Barranco and J. Robert Buchler, Phys. Rev. C **22**, (1980) 1729.
2. H. Müller and B. D. Serot, Phys. Rev. C **52**, (1995) 2072.

3. B. Borderie and J.D. Frankland, *Prog. Part. Nuc. Phys.* **105**, (2019) 82.
4. A. Arcones, G. Martinez-Pinedo, E. O'Connor, A. Schwenk, H.-T. Janka, C. J. Horowitz, and K. Langanke, *Phys. Rev. C* **78**, (2008) 015806.
5. K. Sumiyoshi and G. Röpke, *Phys. Rev. C* **77**, (2008) 055804.
6. T. Fischer, M. Hempel, I. Sagert, Y. Suwa, and J. Schaffner-Bielich, *Eur. Phys. J. A* **50**, (2014) 46.
7. S. Furusawa, H. Nagakura, K. Sumiyoshi, and S. Yamada, *Astrophys. J.* **774**, (2013) 78.
8. S. Furusawa, K. Sumiyoshi, S. Yamada, and H. Suzuki, *Nucl. Phys. A* **957**, (2017) 188.
9. A. Bauswein, S. Goriely, and H.-T. Janka, *Astrophys. J.* **773**, (2013) 78.
10. R. Fernandez, B. D. Metzger, *Mon. Not. Roy. Astro. Soc.* **435**, (2013) 502.
11. O. Just, A. Bauswein, R. A. Pulpillo, S. Goriely, H.-T. Janka, *Mon. Not. Roy. Astro. Soc.* **448**, (2014) 541.
12. D. Ravenhall, C. Pethick, and J. Wilson, *Phys. Rev. Lett.* **50**, (1983) 2066.
13. A. S. Schneider, C. J. Horowitz, J. Hughto, and D. K. Berry, *Phys. Rev. C* **88**, (2013) 065807.
14. C. J. Horowitz, D. K. Berry, C. M. Briggs, M. E. Caplan, A. Cumming, and A. S. Schneider, *Phys. Rev. Lett.* **114**, (2014) 031102.
15. H. Sonoda, G. Watanabe, K. Sato, K. Yasuoka, and T. Ebisuzaki, *Phys. Rev. C* **77**, (2008) 035806, [Erratum: *Phys.Rev.C* **81**, (2010) 049902].
16. S. S. Avancini, S. Chiacchiera, D. P. Menezes, and C. Providência, *Phys. Rev. C* **82**, (2010) 055807, [Erratum: *Phys.Rev.C* **85**, (2012) 059904].
17. S. S. Avancini, M. Ferreira, H. Pais, C. Providência, and G. Röpke, *Phys. Rev. C* **95**, (2017) 045804.
18. F. Ji, J. Hu, S. Bao, and H. Shen, *Phys. Rev. C* **102**, (2020) 015806.
19. Xin-Hui Wu, Si-Bo Wang, Armen Sedrakian, and Gerd Röpke, *J. Low Temp. Phys.* **189**, (2017) 133.
20. A. Sedrakian, *Eur. Phys. J. A* **56**, (2020) 258.
21. T. Fischer *et al.*, arXiv:2008.13608 [astro-ph.HE].
22. S. Rosswog, *Int. J. Mod. Phys. D* **24**, (2015) 1530012.
23. S. S. Avancini, C. C. Barros Jr., D. P. Menezes, and C. Providência, *Phys. Rev. C* **82**, (2010) 025808.
24. S. S. Avancini, C. C. Barros, Jr., L. Brito, S. Chiacchiera, D. P. Menezes, and C. Providência, *Phys. Rev. C* **85**, (2012) 035806.
25. S. Typel, G. Röpke, T. Klähn, D. Blaschke and H. H. Wolter, *Phys. Rev. C* **81**, (2010) 015803.
26. M. Ferreira and C. Providência, *Phys. Rev. C* **85**, (2012) 055811.
27. H. Pais, S. Chiacchiera, and C. Providência, *Phys. Rev. C* **91**, (2015) 055801.
28. S. S. Avancini, M. Ferreira, H. Pais, C. Providência, and G. Röpke, *Phys. Rev. C* **95**, (2017) 045804.
29. H. Pais, F. Gulminelli, C. Providência, and G. Röpke, *Phys. Rev. C* **97** (2018) 045805.
30. H. Pais, F. Gulminelli, C. Providência, and G. Röpke, *Phys. Rev. C* **99**, (2019) 055806.
31. B. G. Todd-Rutel and J. Piekarewicz, *Phys. Rev. Lett.* **95**, (2005) 122501.
32. Y. Sugahara, and H. Toki, *Nucl. Phys. A* **579**, (1994) 557.
33. H. Shen, H. Toki, K. Oyamatsu, and K. Sumiyoshi, *Nucl. Phys. A* **637**, (1998) 435.
34. C. Providência and A. Rabhi, *Phys. Rev. C* **87**, (2013) 055801.
35. S. S. Bao, and H. Shen, *Phys. Rev. C* **89**, (2014) 045807.
36. H. Pais and C. Providência, *Phys. Rev. C* **94**, (2016) 015808.
37. Hong Shen, Fan Ji, Jinniu Hu, and Kohsuke Sumiyoshi, *Astrophys. J.* **891**, (2020) 148.
38. G. A. Lalazissis, J. König, and P. Ring, *Phys. Rev. C* **55**, (1997) 540.
39. C. J. Horowitz and J. Piekarewicz, *Phys. Rev. Lett.* **86**, (2001) 5647.
40. Andrew W. Steiner, Matthias Hempel, and Tobias Fischer, *Astrophys. J.* **774**, (2013) 17.
41. L. Tolos, M. Centelles, and A. Ramos, *Pub. Astron. Soc. Aust.* **34**, (2017) e065.
42. G. A. Lalazissis, T. Nikšić, D. Vretenar, and P. Ring, *Phys. Rev. C* **71**, (2005) 024312.
43. M. Tsang *et al.*, *Phys. Rev. C* **86**, (2012) 015803.
44. J. M. Lattimer and Y. Lim, *Astrophys. J.* **771**, (2013) 51.
45. M. Oertel, M. Hempel, T. Klähn, and S. Typel, *Rev. Mod. Phys.* **89**, (2017) 015007.
46. K. Hebeler, J. Lattimer, C. Pethick, and A. Schwenk, *Astrophys. J.* **773**, (2013) 11.
47. L. Qin, K. Hagel, R. Wada, J. B. Natowitz, S. Shlomo, A. Bonasera, G. Röpke, S. Typel, Z. Chen, M. Huang, *et al.*, *Phys. Rev. Lett.* **108**, (2012) 172701.
48. R. Bougault *et al.*, *J. Phys. G* **47**, (2020) 025103.
49. H. Pais, R. Bougault, F. Gulminelli, C. Providência, *et al.*, *Phys. Rev. Lett.* **125**, (2020) 012701.
50. H. Pais, R. Bougault, F. Gulminelli, C. Providência, *et al.*, *J. Phys. G: Nucl. Part. Phys.* **47**, (2020) 105204.
51. J. B. Natowitz, H. Pais, G. Röpke, *et al.*, arXiv:2009.05200 [nucl-ex].
52. F. Aymard, F. Gulminelli, and J. Margueron, *Phys. Rev. C* **89**, (2014) 065807.
53. F. Gulminelli and Ad. R. Raduta, *Phys. Rev. C* **92**, (2015) 055803.
54. G. Röpke, *Phys. Rev. C* **92**, (2015) 054001.
55. C. Horowitz and A. Schwenk, *Nucl. Phys. A* **776**, (2006) 55.
56. M. Voskresenskaya and S. Typel, *Nucl. Phys. A* **887**, (2012) 42.
57. A. V. Yudin, M. Hempel, S. I. Blinnikov, D. K. Nadyozhin, and I. V. Panov, *Mon. Not. Roy. Astron. Soc.* **483**, (2019) 5426.
58. G. Röpke, *Phys. Rev. C* **101**, (2020) 064310.
59. Olfa Boukari, Helena Pais, Sofija Antić, and Constança Providência, arXiv:2007.08852 [nucl-th].
60. M. Hempel, K. Hagel, J. Natowitz, G. Röpke, and S. Typel, *Phys. Rev. C* **91**, (2015) 045805.